Bifurcations Caused by Feedback between Voltage and Intracellular Ion Concentrations in Ventricular Myocytes

Julian Landaw and Zhilin Qu*
Department of Medicine and Department of Biomathematics, University of California, Los Angeles, California 90095, USA

(Received 6 June 2019; published 21 November 2019)

We develop an iterated map model to describe the bifurcations and complex dynamics caused by the feedback between voltage and intracellular Ca^{2+} and Na^{+} concentrations in paced ventricular myocytes. Voltage and Ca^{2+} can form either a positive or a negative feedback loop, while voltage and Na^{+} form a negative feedback loop. Under certain diseased conditions, when the feedback between voltage and Ca^{2+} is positive, Hopf bifurcations occur, leading to periodic oscillatory behaviors. When this feedback is negative, period-doubling bifurcation routes to alternans and chaos occur.

DOI: 10.1103/PhysRevLett.123.218101

In excitable cells [1], ion concentration gradients across the cell membrane are required for a negative (polarized) resting potential and excitability. The major ions are sodium ion (Na^{+}), potassium ion (K^{+}), and calcium ion (Ca^{2+}), with concentrations in the extracellular space being roughly 140, 4, and 1.5 mM, and in intracellular space being roughly 10 mM, 150 mM, and 100 nM, respectively. These ion gradients are primarily maintained by ion pumps, namely, the Na^{+}-K^{+} pump and the Na^{+}-Ca^{2+} exchange (NCX). During an action potential (AP), Na^{+} and Ca^{2+} enter the cell via voltage-gated Na^{+} channels and Ca^{2+} channels, respectively, and K^{+} exits the cell via K^{+} channels, which then are extruded out or brought into the cell by the pumps, maintaining ion homeostasis of the cell. Since the intracellular ion concentrations affect both ionic currents via ion channels and pumps, feedback loops form between voltage and the ion concentrations. Moreover, the ion channels and different intracellular ion concentration dynamics exhibit distinct timescales. The feedback loops and the multiple timescales can result in very interesting dynamics, such as bursting behaviors seen in many biological cells, including neurons [2–4], pancreatic β cells [2], and cardiac cells [5–7]. Although some of the complex AP dynamics have been understood via bifurcation analyses, much work is still needed to reveal how the feedback and different timescales interact to give rise to these dynamics.

In recent studies [8,9], oscillatory behaviors between APs without early afterdepolarizations (EADs) and APs with EADs have been shown in ventricular myocytes in computer simulations and experiments. It is postulated that this behavior is a result of slow intracellular Na^{+} concentration ($[Na^{+}]_i$) change and feedback between voltage and the ion concentrations of Na^{+} and Ca^{2+}, namely, a positive feedback loop between voltage and intracellular Ca^{2+} concentration ($[Ca^{2+}]_i$) and a negative feedback loop between voltage and $[Na^{+}]_i$. However, a rigorous analysis has not been carried out on how the feedback and multiple timescales give rise to complex dynamics in ventricular myocytes. In this study, we develop a low-dimensional iterated map model that accounts for the different timescales and feedback loops. The iterated map model can accurately capture the complex dynamics of the high-dimensional AP model and reveal the underlying mechanisms and bifurcations, including bistability, Hopf bifurcations, and period-doubling routes to chaos.

To provide insight into the development of the iterated map model and to validate its predictions, we carry out simulations using a detailed ventricular AP model by ten Tusscher *et al.* [10]. The voltage (V) is described by

$$C_m \frac{dV}{dt} = -I_{\text{ion}} + I_{\text{sti}}, \tag{1}$$

where $C_m = 1\ \mu\text{F/cm}^2$ is the membrane capacitance and I_{sti} is the stimulus current density, which is a 2 ms square pulse of amplitude 52 $\mu\text{A/cm}^2$ with a period T. I_{ion} is the total ionic current density, which is composed of many individual ionic currents, i.e., $I_{\text{ion}} = I_{\text{Na}} + I_{\text{K1}} + I_{\text{to}} + I_{\text{Kr}} + I_{\text{Ks}} + I_{\text{Ca,L}} + I_{\text{NCX}} + I_{\text{NaK}} + I_{p\text{Ca}} + I_{p\text{K}} + I_{b\text{Ca}} + I_{b\text{Na}}$. The detailed formualtions of these currents are in the original article by ten Tusscher *et al.* [10]. To generate EADs and the oscillatory action potential duration (APD) dynamics, we made the following modifications: I_{to} and I_{Kr} were removed, the maximum conductance of I_{Ks} was reduced, i.e., $G_{Ks} = 0.125\ \text{mS/cm}^2$, and $I_{\text{Ca,L}}$ was substituted by the formulation by Huang *et al.* [11] with $G_{\text{Ca,L}} = 0.000\,14\ \text{cm}^3/\mu F/s$. We varied the maximum NCX activity (k_{NCX}) to result in different AP dynamics. EADs do not occur under normal conditions but can occur under certain diseased conditions [12], such as long QT syndromes and heart failure. In long QT

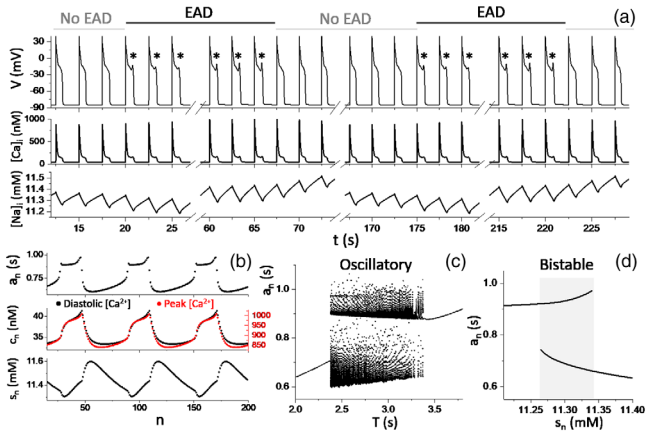

FIG. 1. (a) Voltage, $[Ca^{2+}]_i$, and $[Na^+]_i$ traces showing oscillatory transition between APs with EADs and APs without EADs. Asterisk marks the APs with EADs. $T = 2.5$ s and $k_{NCX} = 5$ nA/pF. (b) a_n, c_n (and peak $[Ca^{2+}]_i$), and s_n versus n from the same simulation in (a). (c) Bifurcation diagram showing APD versus T. 100 APDs are plotted for each T. (d) APD versus s_n for $T = 2.5$ s when $[Na^+]_i$ is clamped at constant values.

syndromes [13,14], one or more (due to gene mutations or drug interactions) of the outward currents are reduced, and in heart failure [15], many of the outward currents are reduced while the NCX activity is enhanced. These alterations promote EADs [16–18] and EAD-related complex nonlinear dynamics [19–21].

Simulations of the AP model show the same oscillatory behavior as in previous studies [8,9]. Figure 1(a) is a voltage trace showing oscillatory transitions between APs with EADs and APs without EADs at $T = 2.5$ s. In this trace, an EAD occurs in each AP from 20 to 67.5 s (total 19 beats), and APD is long. No EAD occurs in the APs from 67.5 to 175 s (total 43 beats), and APD is short. The total length of this combined EAD and no EAD phase is 155 s or 62 beats. This repeats as time goes on, giving rise to a periodic oscillatory behavior. We denote APD of the nth beat as a_n, and $[Ca^{2+}]_i$ and $[Na^+]_i$ at the beginning of this beat as c_n and s_n, respectively. Figure 1(b) shows a_n, c_n, and s_n versus beat number n from the same simulation in Fig. 1(a). The period of oscillation is 62 beats. As APD changes from short to long, both c_n and s_n elevate, and as APD changes from long to short, both c_n and s_n decay. Note that c_n responds much faster than s_n to the APD changes. Figure 1(c) shows a bifurcation diagram plotting a_n versus T, in which the APD is oscillatory between $T = 2.35$ s and $T = 3.4$ s, but stable for smaller or larger T outside this region. We also carried out simulations by clamping $[Na^+]_i$ at different levels [Fig. 1(d)], revealing that APD is bistable. This bistable phenomenon agrees with the results from previous studies [8,9].

To reveal the bifurcations that lead to this behavior and other dynamics caused by the feedback and timescales, we developed an iterated map model to describe the dynamics of a_n, c_n, and s_n. The equations of the iterated maps are

$$a_n = g(c_n, s_n)\,, \tag{2}$$

$$c_{n+1} - \bar{c} = (1 - \beta_c)(c_n - \bar{c}), \tag{3}$$

$$s_{n+1} - \bar{s} = (1 - \beta_s)(s_n - \bar{s}). \tag{4}$$

Equation (2) describes the dependence of a_n on c_n and s_n. Equations (3) and (4) describe the dependences of c_{n+1} and s_{n+1} on their values in the previous beat with $\bar{c} = \bar{c}(a_n, T)$ and $\bar{s} = \bar{s}(a_n, T)$ being their steady states under constant a_n and T. β_c and β_s are two parameters determining how fast c_n and s_n approach their steady states. When $\beta_c = 1$ or $\beta_s = 1$, c_n or s_n instantaneously reaches its steady state. When $\beta_c = 0$ or $\beta_s = 0$, c_n or s_n will never reach its steady state, which corresponds to the case of holding the concentration constant or clamped. Since s_n changes much more slowly than c_n [see e.g., Fig. 1(b)], $\beta_s \ll \beta_c$; therefore,

$$0 < \beta_s \ll \beta_c < 1. \tag{5}$$

We used $\beta_c = 0.32$ and $\beta_s = 0.01$ unless specified.

The rationale for choosing linear iterated map equations for c_n and s_n is as follows: for a fixed T, after a sudden shortening of APD, the ion concentration decays exponentially toward a new steady state [22]. Based on our simulations, the steady state concentrations increase with APD but decrease with T. We have the following equations for $\bar{c}$ and $\bar{s}$:

$$\bar{c} = c_1(T)a_n + c_0 = \frac{0.2}{T + 2.1}a_n + c_0\,, \tag{6}$$

$$\bar{s} = s_1(T)a_n + s_0 = \frac{0.03}{T + 2.8}a_n + s_0\,, \tag{7}$$

where c_0 and s_0 are their values for $T \to \infty$, corresponding to the cell in quiescence. We set $c_0 = 0$ and $s_0 = 7$ mM.

A key step is to define the function g in Eq. (2). As shown in our previous study [22], when $[Na^+]_i$ is clamped at a constant, g is a sole function of c_n, and thus is one dimensional. However, here g is a two-dimensional function depending on both c_n and s_n, which becomes nontrivial to be defined. To gain insight into how a_n depends on c_n and s_n, we plot a_n (in color scale) versus c_n and s_n in Fig. 2(a) using the data from the simulations shown in Fig. 1. In a wide range of c_n and s_n, the iso-APD contour lines are almost linear, indicating that if one uses the following transformation:

$$z_n = s_n + \alpha c_n\,, \tag{8}$$

the two-dimensional function may be reduced into a one dimensional one as

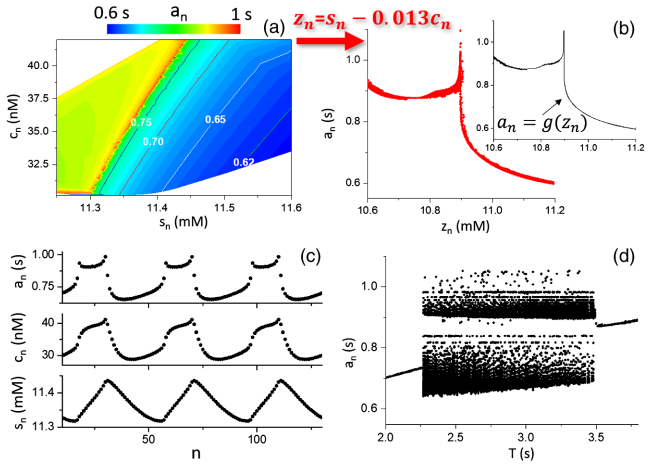

FIG. 2. (a) a_n (color scale) versus s_n and c_n from the simulation data from Fig. 1. (b) a_n versus z_n after the transform $z_n = s_n - 0.013c_n$. Inset (black) is a piecewise linear function based on the data. (c) a_n, c_n, and s_n versus n from the iterated map model using the g function in the inset in (b). (d) Bifurcation diagram showing a_n versus T from the iterated map model.

$$a_n = g(z_n). \tag{9}$$

Figure 2(b) replots the data of Fig. 2(a) using $z_n = s_n - 0.013c_n$. Under this transformation, the data points indeed fall in a very narrow band, indicating that Eq. (9) can well describe the data.

Since both $\bar{c}$ and $\bar{s}$ are positively related to a_n [see Eqs. (6) and (7)], whether the feedback loops between APD and $[Na^+]_i$ and $[Ca^{2+}]_i$ are positive or negative is determined by the dependence of a_n on c_n and s_n. In ventricular myocytes, in general, a higher $[Na^+]_i$ gives rise to a smaller APD since a higher $[Na^+]_i$ results in a larger I_{NaK} and a smaller I_{NCX}, and thus a_n depends on s_n negatively. This results in a negative feedback loop between APD and $[Na^+]_i$. However, the relation between APD and $[Ca^{2+}]_i$ is more complex. APD can either negatively or positively depend on $[Ca^{2+}]_i$. By the way we choose z_n in Eq. (8), a_n negatively depends on z_n [note that the data in Fig. 2(b) are nonmonotonic], so $\alpha < 0$ means a_n depends on c_n positively, indicating that the feedback between APD and $[Ca^{2+}]_i$ is positive. $\alpha > 0$ means a_n depends on c_n negatively, indicating that the feedback between APD and $[Ca^{2+}]_i$ is negative.

To examine if the iterated map model can capture the dynamics of the AP model, we obtained a g function [inset of Fig 2(b)] using a linear interpolation of points manually chosen in the data set in Fig. 2(b) to assure a one-to-one correspondence between a_n and z_n. We then used this linearly interpolated function for simulations of the iterated map model. Figure 2(c) shows a_n, c_n, and s_n versus n for $T = 2.5$ s and Fig. 2(d) shows a bifurcation diagram by plotting a_n versus T. These results closely match those of the AP model shown in Figs. 1(b) and 1(c), indicating that the low-dimensional iterated map model can accurately capture the dynamics of the high-dimensional AP model.

We then used the iterated map model to perform stability and bifurcation analyses. Note that only two equations of the three equations are free, and one can easily eliminate a_n by substituting a_n in Eqs. (3) and (4) using Eq. (2) [or Eq. (9)]. The Jacobian matrix J for Eqs. (3) and (4) is

$$J = \begin{pmatrix} 1 - \beta_c + c_1\alpha\beta_c g' & c_1\beta_c g' \\ s_1\alpha\beta_s g' & 1 - \beta_s + s_1\beta_s g' \end{pmatrix}, \tag{10}$$

where $g' = dg/dz$. Defining $\tau = \mathrm{tr}(J)$ and $\Delta = \det(J)$ to be the trace and determinant of J, then the two eigenvalues are $\lambda = (\tau \pm \sqrt{\tau^2 - 4\Delta})/2$. Although the function g obtained from the AP model is nonmonotonic, for simplicity, we assume that g in general is a decreasing function of z_n such that

$$g' < 0 \tag{11}$$

always holds, such as in a descending Hill function [e.g., Eq. (17)]. Using this Jacobian combined with the conditions of Eqs. (5) and (11), one obtains the following bifurcations and stability criteria:

(1) $\tau^2 - 4\Delta < 0$, *Hopf bifurcation.*—In this case, the eigenvalues are a pair of complex conjugates, i.e., $\lambda = [\tau \pm i\sqrt{-(\tau^2 - 4\Delta)}]/2$. When $|\lambda| = \sqrt{\Delta} > 1$, instability occurs via a Hopf bifurcation, which leads to the following stability criterion:

$$[s_1\beta_s(1 - \beta_c) + c_1\alpha\beta_c(1 - \beta_s)]g' > \beta_c + \beta_s + \beta_c\beta_s. \tag{12}$$

A special case is when $\beta_s = 0$, corresponding to $[Na^+]_i$ being clamped at a constant. Under this condition, the stability criterion in Eq. (12) simplifies to

$$c_1\alpha g' > 1. \tag{13}$$

This is exactly the condition for bistability to occur in the system when $[Na^+]_i$ is clamped, which can be obtained by setting s_n to a constant in Eqs. (2)–(4). Since $g' < 0$, and thus $\alpha < 0$ (or a positive feedback loop between APD and $[Ca^{2+}]_i$) is required for bistability to occur. This stability boundary is plotted as the red dashed line in Fig. 3. We also plotted the stability boundaries for $\beta_s = 0.01$ and $\beta_s = 0.2$ in red solid lines. A larger β_s requires a steeper g function for the Hopf bifurcation to occur, indicating that a faster $[Na^+]_i$ accumulation rate suppresses this instability. Positive feedback between APD and $[Ca^{2+}]_i$ is always required ($\alpha < 0$) for a Hopf bifurcation.

(2) $\tau^2 - 4\Delta > 0$, *period-doubling bifurcation.*—In this case, the two eigenvalues are real and when the smaller one $\lambda = (\tau - \sqrt{\tau^2 - 4\Delta})/2 < -1$, or $\tau + 2 < \sqrt{\tau^2 - 4\Delta}$, instability occurs via a period-doubling bifurcation, which leads to the following stability criterion:

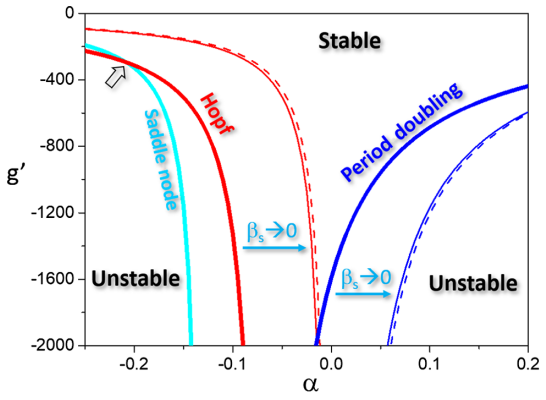

FIG. 3. Stability boundaries of the steady state in the g'-α space. $\beta_c = 0.32$ and $T = 2.5$ s. Blue lines are the boundaries for period-doubling bifurcation for $\beta_s = 0.2$ (thick solid), $\beta_s = 0.01$ (thin solid), and $\beta_s = 0$ (dashed). Red lines are the boundaries for Hopf bifurcation for $\beta_s = 0.2$ (thick solid), $\beta_s = 0.01$ (thin solid), and $\beta_s = 0$ (dashed). The cyan line is the boundary for saddle-node bifurcation. The steady state is stable above but unstable below these boundaries. The open arrow indicates the intersection of the Hopf and saddle-node bifurcations.

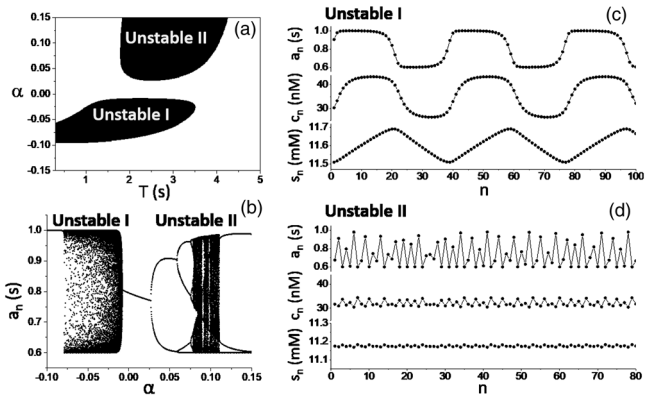

FIG. 4. (a) Unstable regions in α-T space, obtained from the iterated map model using the Hill function Eq. (17). (b) Bifurcation diagrams showing a_n versus α using the iterated map model for $T = 2.5$ s. (c) An example of oscillatory behavior from unstable region I with $\alpha = -0.015$. (d) An example of chaotic behavior from unstable region II with $\alpha = 0.1$. Note: We alter k_{NCX} to alter the behavior of the AP model (see Fig. 5), which changes not only the α value but also the value of k_d [e.g., compare Fig. 2(b) to Fig. 5(b)]. To match the bifurcation behaviors, we set k_d as a function of α, i.e., $k_d = 11.5 + 28\alpha$.

$$[s_1\beta_s(2-\beta_c) + c_1\alpha\beta_c(2-\beta_s)]g' < -(2-\beta_c)(2-\beta_s) \tag{14}$$

When $\beta_s = 0$, Eq. (14) becomes

$$c_1\alpha\beta_c g' < -2 + \beta_c\,, \tag{15}$$

which is the blue dashed line in Fig. 3. We also plotted the stability boundaries for $\beta_s = 0.01$ and $\beta_s = 0.2$ in blue solid lines. A larger β_s requires a less steep g function for the period-doubling bifurcation to occur, indicating a faster $[\mathrm{Na}^+]_i$ accumulation rate promotes this instability. This instability mainly occurs when $\alpha > 0$, i.e., when the feedback between APD and $[\mathrm{Ca}^{2+}]_i$ is negative.

(3) $\tau^2 - 4\Delta > 0$, *saddle-node bifurcation.*—In this case, when the larger of the two eigenvalues $\lambda = (\tau + \sqrt{\tau^2 - 4\Delta})/2 > 1$, or $2 - \tau < \sqrt{\tau^2 - 4\Delta}$, instability occurs via a saddle-node bifurcation, leading to the condition

$$(s_1 + c_1\alpha)g' > 1. \tag{16}$$

Note that Eq. (16) is independent of β_c and β_s. As shown in Fig. 3, this stability boundary is below the boundary of Hopf bifurcation, and one only observes the Hopf bifurcation induced oscillatory behavior. But bistability can be observed when the stability boundary is above the boundary of Hopf bifurcation (open arrow in Fig. 3) when α is more negative and the $[\mathrm{Na}^+]_i$ change is relatively fast ($\beta_s > 0.2$). This is unlikely in ventricular myocytes since $[\mathrm{Na}^+]_i$ accumulates or decays very slowly and thus β_s is small, on the order of 0.01.

For more detailed theoretical analyses and computer simulations using the map model, we use a Hill function for g in Eq. (9) as

$$a_n = g(z_n) = a_{\min} + \frac{a_{\max} - a_{\min}}{1 + (\frac{z_n}{k_d})^h}\,. \tag{17}$$

Based on Fig. 2(b), we chose $a_{\max} = 1$ s, $a_{\min} = 0.6$ s, and $h = 500$. k_d is the dissociation constant of the Hill function.

With the analytical function Eq. (17), one can easily obtain the steady state of the map model. Using Eqs. (3), (6), and (17), one obtains for the steady state (c_s) of c_n as

$$c_s = \frac{0.2}{T + 2.1}\left[a_{\min} + \frac{a_{\max} - a_{\min}}{1 + (\frac{s_n + \alpha c_s}{k_d})^h}\right] + c_0\,. \tag{18}$$

If s_n is clamped at a certain constant, the solution of Eq. (18) can be bistable when $\alpha < 0$, agreeing with the results of the AP model [Fig. 1(c)]. Figure 4 shows results of the map model using the g function in Eq. (17). Figure 4(a) shows the unstable regions in the α-T space, showing an unstable region when $\alpha < 0$ (unstable I) and another when $\alpha > 0$ (unstable II). Figure 4(b) shows a bifurcation diagram across the two unstable regions for $T = 2.5$ s. In unstable region I, only periodic oscillatory behavior is observed [Fig. 4(c)]. In unstable region II, period-doubling routes to chaos occur, leading to high periodicity and chaos [Fig. 4(d)]. Compared to unstable region I, even though APD varies in roughly the same

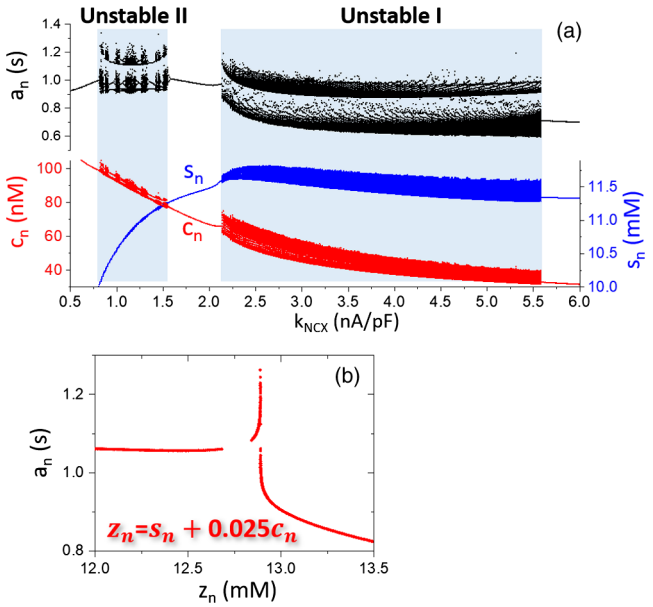

FIG. 5. (a) Bifurcation diagrams showing a_n, c_n, and s_n versus k_{NCX} in the AP model for $T = 2.5$ s. (b) a_n versus z_n for $k_{\mathrm{NCX}} = 1$ nA/pF using the transform $z_n = s_n + 0.025c_n$.

range, the $[Ca^{2+}]_i$ variation is attenuated and $[Na^+]_i$ exhibits a very small variation.

One can change the feedback from positive to negative and thus the dynamical behaviors in the AP model by altering k_{NCX}. Figure 5(a) shows the AP dynamics vesus k_{NCX} for $T = 2.5$ s, which shows the same bifurcations as in Fig. 4(b). When k_{NCX} is in the range from 0.75 to 1.5 nA/pF, period-doubling routes to chaos occur, intermingled with periodic windows, corresponding to unstable region II in Fig. 4. If we plot a_n against z_n using the transform Eq. (8), $\alpha > 0$ is needed [Fig. 5(b)], indicating that the feedback between APD and $[Ca^{2+}]_i$ is indeed negative. After a stable region for k_{NCX} between 1.5 to 2.1 nA/pF, another unstable region (from 2.1 to 5.6 nA/pF) occurs. Periodic oscillations occur in this whole region, corresponding to unstable region I in Fig. 4. In this region, the feedback between APD and $[Ca^{2+}]_i$ is always positive [$\alpha < 0$, as in Fig. 2(b)]. Also agreeing with the map results shown in Fig. 4, the APD variations are in the same range in the two regions, but the $[Ca^{2+}]_i$ and $[Na^+]_i$ varations are different. In unstable region II, the $[Ca^{2+}]_i$ variation is attenuated, and $[Na^+]_i$ exhibits almost no variation.

In conclusion, the iterated map model incorporating the multiple timescales and the feedback between APD and $[Ca^{2+}]_i$ and $[Na^+]_i$ can well describe the bifurcations and complex dynamics in paced ventricular myocytes. Specifically, under diseased conditions in which EADs are present and the feedback between APD and $[Ca^{2+}]_i$ is positive, Hopf bifurcations occur, leading to periodic oscillatory behaviors. When this feedback is negative, period-doubling bifurcation routes to alternans and chaos occur. The bifurcations from the map model may provide mechanistic insight into slow time course or delay (or memory) induced period doubling [23] and oscillations [8,24] shown in experiments. Differing from many previous theoretical studies [24–28] on the effects of memory, our iterated map model incorporates the specific feedback loops and timescales of $[Ca^{2+}]_i$ and $[Na^+]_i$ accumulation, which reveals the bifurcations leading to the complex AP dynamics in ventricular myocytes caused by feedback between APD and $[Ca^{2+}]_i$ and $[Na^+]_i$. These cellular AP dynamics may play important roles in cardiac arrhythmogenesis in cardiac tissue [29].

This study was supported by NIH Grants No. R01 HL134709, No. R01 HL139829, No. T32 GM00 8042, and No. F30 HL140864.

*zqu@mednet.ucla.edu.

[1] B. Hille, *Ion Channels of Excitable Membranes*, 3rd ed. (Sinauer Associates, Inc., Sunderland, Massachusetts, USA, 2001).
[2] J. P. Keener and J. Sneyd, *Mathematical Physiology*, Interdisciplinary Applied Mathematics (Springer, New York, 1998).
[3] C. A. Del Negro, C. F. Hsiao, S. H. Chandler, and A. Garfinkel, Biophys. J. **75**, 174 (1998).
[4] A. Shilnikov, R. L. Calabrese, and G. Cymbalyuk, Phys. Rev. E **71**, 056214 (2005).
[5] A. M. Kunysz, A. Shrier, and L. Glass, Am. J. Physiol. Cell Physiol. **273**, C331 (1997).
[6] A. G. Torrente, R. Zhang, A. Zaini, J. F. Giani, J. Kang, S. T. Lamp, K. D. Philipson, and J. I. Goldhaber, Proc. Natl. Acad. Sci. U.S.A. **112**, 9769 (2015).
[7] P. Glynn, B. Onal, and T. J. Hund, PLoS One **9**, e89049 (2014).
[8] Y. Xie, Z. Liao, E. Grandi, Y. Shiferaw, and D. M. Bers, Circ. Arrhythm. Electrophysiol. **8**, 1472 (2015).
[9] T. Krogh-Madsen and D. J. Christini, Chaos **27**, 093907 (2017).
[10] K. H. ten Tusscher, D. Noble, P. J. Noble, and A. V. Panfilov, Am. J. Physiol. Heart Circ. Physiol. **286**, H1573 (2004).
[11] X. Huang, T. Y. Kim, G. Koren, B.-R. Choi, and Z. Qu, Am. J. Physiol. Heart Circ. Physiol. **311**, H1470 (2016).
[12] Z. Qu, L.-H. Xie, R. Olcese, H. S. Karagueuzian, P.-S. Chen, A. Garfinkel, and J. N. Weiss, Cardiovasc. Res. **99**, 6 (2013).
[13] H. Morita, J. Wu, and D. P. Zipes, Lancet **372**, 750 (2008).
[14] D. M. Roden, N. Engl. J. Med. **350**, 1013 (2004).
[15] G. F. Tomaselli and E. Marban, Cardiovasc. Res. **42**, 270 (1999).
[16] C. E. Clancy and Y. Rudy, Nature (London) **400**, 566 (1999).
[17] N. Vandersickel, I. V. Kazbanov, A. Nuitermans, L. D. Weise, R. Pandit, and A. V. Panfilov, PLoS One **9**, e84595 (2014).

[18] E. Pueyo, A. Corrias, L. Virág, N. Jost, T. Szél, A. Varró, N. Szentandrássy, P. P. Nánási, K. Burrage, and B. Rodríguez, Biophys. J. **101**, 2892 (2011).
[19] D. X. Tran, D. Sato, A. Yochelis, J. N. Weiss, A. Garfinkel, and Z. Qu, Phys. Rev. Lett. **102**, 258103 (2009).
[20] D. Sato, L. H. Xie, T. P. Nguyen, J. N. Weiss, and Z. Qu, Biophys. J. **99**, 765 (2010).
[21] D. Sato, L.-H. Xie, A. A. Sovari, D. X. Tran, N. Morita, F. Xie, H. Karagueuzian, A. Garfinkel, J. N. Weiss, and Z. Qu, Proc. Natl. Acad. Sci. U.S.A. **106**, 2983 (2009).
[22] J. Landaw and Z. Qu, Phys. Rev. E **97**, 042414 (2018).
[23] J. Sun, F. Amellal, L. Glass, and J. Billette, J. Theor. Biol. **173**, 79 (1995).
[24] N. F. Otani and R. F. Gilmour, J. Theor. Biol. **187**, 409 (1997).
[25] N. F. Otani, Chaos **27**, 093935 (2017).
[26] J. Landaw, A. Garfinkel, J. N. Weiss, and Z. Qu, Phys. Rev. Lett. **118**, 138101 (2017).
[27] E. G. Tolkacheva, D. G. Schaeffer, D. J. Gauthier, and W. Krassowska, Phys. Rev. E **67**, 031904 (2003).
[28] J. J. Fox, E. Bodenschatz, and R. F. Gilmour, Phys. Rev. Lett. **89**, 138101 (2002).
[29] Z. Qu, G. Hu, A. Garfinkel, and J. N. Weiss, Phys. Rep. **543**, 61 (2014).